Turbulence statistics in a high Mach number boundary layer downstream of an incident shock wave

By L. Fu, M. Karp, S. T. Bose,
P. Moin AND J. Urzay

1. Motivation and objectives

Unlike subsonic vehicles, where the boundary layer over the geometry surface is mostly turbulent and adiabatic, the surface temperature of vehicles flying at hypersonic or highly supersonic speeds typically is significantly lower than the stagnation temperature with considerable cooling on the surface. Consequently, the prediction of the heat flux between the turbulent boundary layer and the vehicle surface is vital for designing the thermal protection system of hypersonic vehicles (Urzay 2018), which, however, relies on an in-depth understanding of the flow physics of highly compressible turbulent boundary layers.

While compressible turbulent boundary layers are substantially more complicated than incompressible boundary layers, the complexity can be greatly reduced by developing certain transformations that convert compressible turbulent boundary layer data into incompressible boundary layer data. Morkovin (1962) proposed that, for Mach numbers less than 5, any difference between compressible turbulent boundary layers and incompressible boundary layers can be accounted for by incorporating the variations of mean fluid quantities, because the dilatation effects are negligible. Many transformations and scaling laws have been developed on the basis of Morkovin's hypothesis; for example, the van Driest transformation (van Driest 1956) converts the compressible mean velocity profile into the universal log-law in the incompressible limit. However, despite the success of Morkovin's hypothesis (Morkovin 1962) and the van Driest transformation (van Driest 1956) for adiabatic turbulent boundary layers, verified by both experiments and direct numerical simulation (DNS) data (e.g. Fernholz & Finley 1980; Guarini *et al.* 2000; Pirozzoli *et al.* 2004; Trettel & Larsson 2016), their validity is still not well understood for non-adiabatic hypersonic or highly supersonic boundary layers due to the limited data available. Recent research includes numerical investigations of hypersonic temporally evolving turbulent boundary layers incorporating the effects of wall temperature (Duan *et al.* 2010), Mach number (Duan *et al.* 2011), and high enthalpy (Duan & Martin 2011).

In this work, the turbulence statistics in highly supersonic boundary layers downstream of an incident shock wave are investigated by DNS. The objective is to examine the transformations and scaling laws of spatially evolving highly supersonic boundary layers with a canonical setup. This can allow for the development of efficient reduced-order models for turbulent boundary layers, such as wall-modeled large-eddy simulations (WMLES) (see, e.g., Bose & Park 2018). The rest of this brief is organized as follows: In Section 2, the computational setup and the flow solver are briefly described. Detailed analyses of the turbulence statistics are given in Section 3. Concluding remarks are given in the last section.

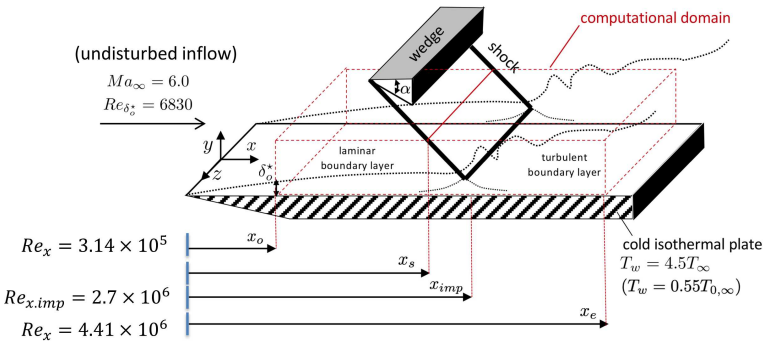

FIGURE 1. Sketch of the computational setup for shock/boundary layer interactions.

2. Computational setup

Our setup corresponds to DNS of shock/boundary layer interactions at various shock angles as detailed by Fu *et al.* (2018). In the current study, we focus on the turbulent boundary layers, downstream of the shock impingement, with the aim of examining known correlations and scaling laws. The geometry and operating conditions correspond to the ones explained by Sandham *et al.* (2014). Specifically, air at $Ma_\infty = 6.0$ flows over an isothermal flat plate held at temperature $T_w = 4.5T_\infty$, as schematically shown in Figure 1. A wedge held above the plate is responsible for generating the shock wave that impinges on the boundary layer with the impingement location $(x - x_o)/\delta_o^\star = 350$ and $Re_{x,imp} = 2.7 \times 10^6$, where Re is defined on the free-stream velocity and viscosity and $\delta_o^\star$ is the displacement thickness at the inflow. In this work, three wedge angles of $\alpha = 6°$, $7°$, and $8°$ are studied, while all other parameters are kept constant.

The second-order-accurate, finite-volume code CharLES (Bres *et al.* 2018), which solves the compressible Navier-Stokes equations in conservative form, is employed in the present simulations. The numerical method consists of an approximately entropy-preserving scheme that deploys the necessary numerical dissipation in the vicinity of shocks based on an artificial viscosity paradigm. The governing equations are supplemented with Sutherland's law for the dynamic viscosity under a constant molecular Prandtl number $Pr = 0.72$ (with Sutherland's model constants satisfying $T_{\text{ref}} = T_\infty$ and $S/T_\infty = 1.69$), the ideal-gas equation of state, and the assumption of a calorically perfect gas with $\gamma = 1.4$.

The dimensions of the computational domain are $600\delta_o^\star \times 75\delta_o^\star \times 45\delta_o^\star$ in the streamwise, wall-normal, and spanwise directions, respectively. The grids employed are Cartesian with stretching in the vertical direction, and the resolution is $6000 \times 600 \times 400$ (1.44 billion cells). The near-wall resolution close to the outlet in viscous units is listed in Table 1 for each case. Table 2 provides the values of the Reynolds number Re_θ, Re_τ, edge Mach number Ma_e (the subscript e denotes the boundary layer edge), the Stanton number, and T_e/T_w at the streamwise station $(x - x_o)/\delta_o^\star = 580$ with local $Re_x = 4.27 \times 10^6$. In all cases in Table 2, the edge Mach number Ma_e of the turbulent boundary layer is smaller than the inflow free-stream Mach number $Ma_\infty = 6$ (highly supersonic rather than hypersonic). The boundary layers at station $(x - x_o)/\delta_o^\star = 580$ for all three wedge angles are fully turbulent.

wedge angle α (deg)	DNS first-cell resolution $\Delta x^+ \times \Delta y^+ \times \Delta z^+$ [–]
6	$5.63 \times 1.35 \times 6.33$
7	$6.51 \times 1.56 \times 7.32$
8	$7.46 \times 1.79 \times 8.40$

TABLE 1. Maximum grid resolution near the wall in viscous units ν_w/u_τ at the outlet plane, where ν_w is the kinematic viscosity at the wall and $u_\tau = \sqrt{\tau_w/\rho_w}$ is the friction velocity based on the wall shear stress τ_w and the density at the wall ρ_w.

wedge angle α (deg)	Re_θ	Re_τ	Ma_e	St	T_e/T_w
6	$2,796$	595.13	4.5	3.61×10^{-3}	0.365
7	$2,846$	682.42	4.2	3.88×10^{-3}	0.402
8	$2,912$	787.88	4.0	4.36×10^{-3}	0.435

TABLE 2. Reynolds number based on momentum thickness Re_θ, Reynolds number based on wall friction velocity Re_τ, edge Mach number Ma_e, Stanton number St, and T_e/T_w at the streamwise station $(x - x_o)/\delta_o^\star = 580$.

3. Results

3.1. *Velocity scaling laws*

To assess the mean velocity profile in fully turbulent compressible boundary layers, we consider the van Driest transformation (van Driest 1956)

$$\begin{cases} y_{vD}^+ = y^+, \\ u_{vD}^+ = \int_0^{u^+} \left(\frac{\langle\rho\rangle}{\rho_w}\right)^{0.5} du^+, \end{cases} \tag{3.1}$$

which accounts for density variation effects, with $\langle\rangle$ denoting the time- and spanwise-averaging operator and the subscript w indicating quantities at the wall, as well as the transformation of Trettel & Larsson (2016)

$$\begin{cases} y^* = \frac{\langle\rho\rangle(\tau_w/\langle\rho\rangle)^{0.5} y}{\langle\mu\rangle}, \\ u_{TL}^+ = \int_0^{u^+} \left(\frac{\langle\rho\rangle}{\rho_w}\right)^{0.5} [1 + \frac{1}{2}\frac{1}{\langle\rho\rangle}\frac{d\langle\rho\rangle}{dy} y - \frac{1}{\langle\mu\rangle}\frac{d\langle\mu\rangle}{dy} y] du^+, \end{cases} \tag{3.2}$$

which further accounts for the wall heating/cooling effects.

Figure 2 shows the mean velocity profiles on a logarithmic scale with both transformations for $\alpha = 6°$, $7°$, and $8°$. In contrast to the investigations reported for channel flows with cold walls (Trettel & Larsson 2016), the transformed velocity profiles do not collapse perfectly with the incompressible log-law in the log layer. The failure of this collapse is also reported for the shock/boundary layer interactions with Mach number $M_\infty = 2.28$ by Volpiani *et al.* (2018). In agreement with findings by Zhang *et al.* (2018), the stronger

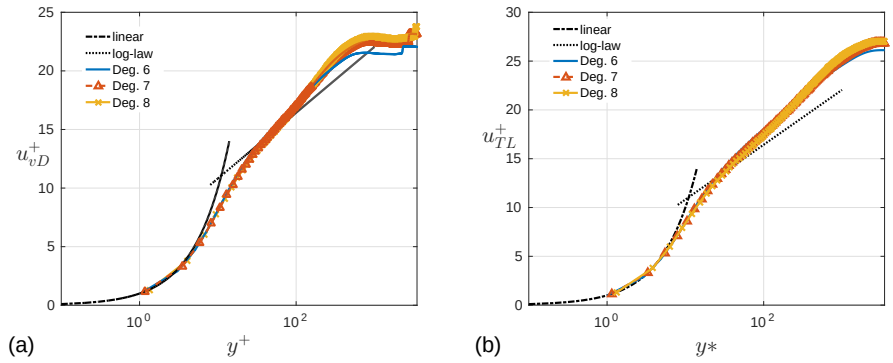

FIGURE 2. Assessment of the boundary layer at the streamwise station $(x - x_o)/\delta_o^\star = 580$: van Driest-transformed mean velocity u^+_{vD} plotted versus y^+ (a) and Trettel-Larsson-transformed u^+_{TL} plotted versus the semilocally scaled y^* (b). The linear relation $u^+ = y^+$ and the incompressible log-law $u^+ = 2.44 \ln y^+ + 5.2$ are also plotted for comparison.

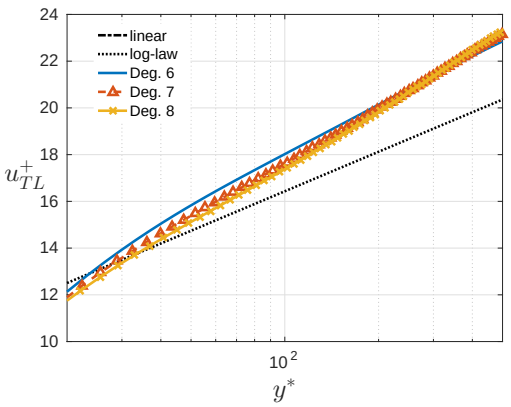

FIGURE 3. Zoomed-in view of Figure 2(b).

the wall cooling is (i.e., the higher Ma is for a fixed value of T_w), the smaller is the effective von Kármán constant of the expected log profiles, as can be seen in Figure 3.

3.2. *Mean temperature-velocity relation*

Reynolds (1874) was the first to present a mean temperature-velocity relationship for incompressible wall-bounded flows through the similarity between the Reynolds-averaged momentum and energy equations. Later, by assuming a Prandtl number of unity and utilizing the similarity between the total enthalpy and the velocity, Crocco (1932) and Busemann (1931) independently derived a relationship for compressible boundary layers, with which the mean temperature is a quadratic function of the mean velocity as

$$\frac{\bar{T}}{\bar{T}_e} = \frac{\bar{T}_w}{\bar{T}_e} + \frac{\bar{T}_{te} - \bar{T}_w}{\bar{T}_e}\left(\frac{\bar{u}}{\bar{u}_e}\right) + \frac{\bar{T}_e - \bar{T}_{te}}{\bar{T}_e}\left(\frac{\bar{u}}{\bar{u}_e}\right)^2, \tag{3.3}$$

where $\bar{T}$ and $\bar{u}$ denote the mean temperature and streamwise velocity, respectively. The stagnation temperature is given by $\bar{T}_{te} = \bar{T}_e + \bar{u}_e^2/(2C_p)$, where C_p is the specific heat capacity at constant pressure. In order to account for the deviation of the Prandtl number

Cases	sPr	θ	Deviation
Deg. 6	0.83304	0.8259	0.9%
Deg. 7	0.81144	0.8259	1.75%
Deg. 8	0.81	0.8259	1.93%

TABLE 3. The statistics of sPr, measured at the streamwise station $(x - x_o)/\delta_o^\star = 580$.

from unity, Walz (1962) developed the following mean temperature-velocity relation

$$\frac{\bar{T}}{\bar{T}_e} = \frac{\bar{T}_w}{\bar{T}_e} + \frac{\bar{T}_r - \bar{T}_w}{\bar{T}_e}\left(\frac{\bar{u}}{\bar{u}_e}\right) + \frac{\bar{T}_e - \bar{T}_r}{\bar{T}_e}\left(\frac{\bar{u}}{\bar{u}_e}\right)^2, \tag{3.4}$$

by introducing a recovery temperature $\bar{T}_{te} = \bar{T}_e + r\bar{u}_e^2/(2C_p)$ with the recovery factor $r \approx 0.9$ (Volpiani *et al.* 2018). Although Walz's relation improves the prediction of the Crocco-Busemann formula significantly for compressible boundary layers with an adiabatic wall, its performance for compressible boundary layers with a non-adiabatic wall is unsatisfactory (Zhang *et al.* 2014). Duan & Martin (2011) alleviate the dependence of the performance on the thermal wall condition by defining a dimensionless recovery enthalpy and fitting to a wide range of DNS data, leading to the following modified temperature-velocity relation

$$\frac{\bar{T}}{\bar{T}_e} = \frac{\bar{T}_w}{\bar{T}_e} + \frac{\bar{T}_r - \bar{T}_w}{\bar{T}_e} f\left(\frac{\bar{u}}{\bar{u}_e}\right) + \frac{\bar{T}_e - \bar{T}_r}{\bar{T}_e}\left(\frac{\bar{u}}{\bar{u}_e}\right)^2, \tag{3.5}$$

where the function $f(\bar{u}/\bar{u}_e)$ is defined as

$$f(\frac{\bar{u}}{\bar{u}_e}) = (1-\theta)\left(\frac{\bar{u}}{\bar{u}_e}\right)^2 + \theta\left(\frac{\bar{u}}{\bar{u}_e}\right),\ \theta = 0.8259. \tag{3.6}$$

Figure 4 shows the mean temperature-velocity relation for $\alpha = 6°$, $7°$, and $8°$. The predictions from the Crocco-Busemann relation, Walz's relation, and the Duan-Martin model are also compared. For all three cases, while Walz's relation performs much better than the Crocco-Busemann relation, Walz's prediction still deviates from the DNS data remarkably and the maximum discrepancy occurs at $\bar{u} = 40\%\bar{u}_e$, which is similar to the observations by Zhang *et al.* (2014) and Duan *et al.* (2010) for high-Mach-number turbulent boundary layers with cold walls. In contrast, the Duan-Martin predictions (Duan & Martin 2011) show excellent agreement with the DNS data. Based on the concept of generalized strong Reynolds analogy (SRA), Zhang *et al.* (2014) derive the constant θ in Eq. (3.6) as sPr, which equals $(\bar{u}_e/(\bar{T}_r - \bar{T}_w))(\partial\bar{T}/\partial\bar{u})\big|_w$. As shown in Table 3, the discrepancy between the prediction of Zhang *et al.* (2014) and the data fitting of Duan & Martin (2011) is less than 2% for all three cases.

3.3. *Strong Reynolds analogy*

Morkovin (1962) first identified a set of relations between the streamwise velocity fluctuation u' and the temperature fluctuation T', known as the SRA. By neglecting the total temperature fluctuations and assuming a Prandtl number of unity, the SRA relation is derived for the zero-pressure-gradient adiabatic turbulent boundary layers as

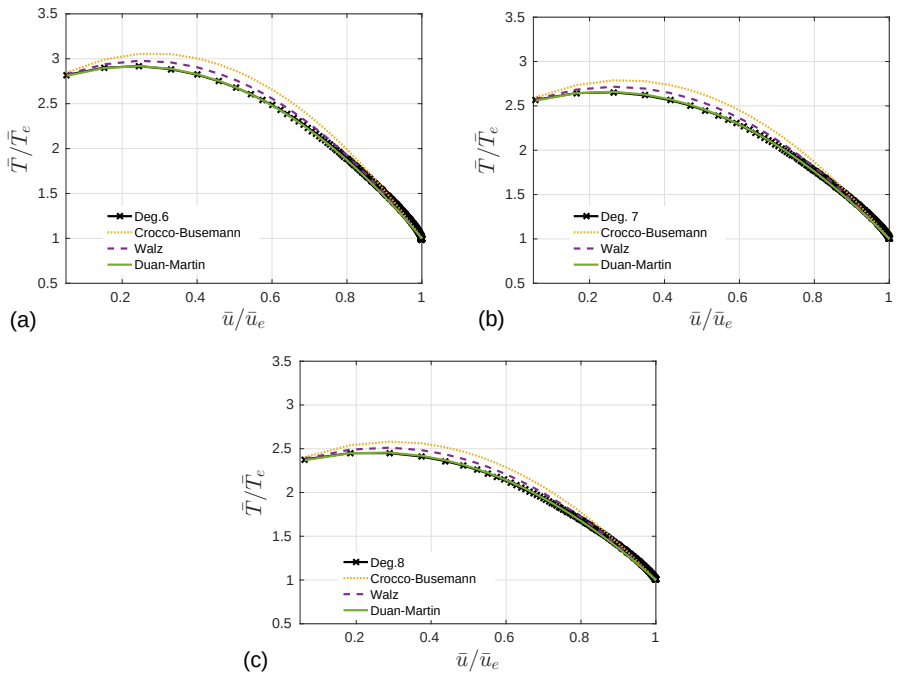

FIGURE 4. Mean temperature-velocity relation at the streamwise station $(x - x_o)/\delta_o^\star = 580$ for $\alpha = 6^\circ$ (a), 7° (b), and 8° (c). The dotted line corresponds to data from Crocco (1932) and Busemann (1931), the dashed line to Walz (1962), and the solid line to Duan & Martin (2011).

$$\frac{\sqrt{\overline{T'^2}}}{\overline{T}} = (\gamma - 1)M^2 \frac{\sqrt{\overline{u'^2}}}{\overline{u}}, \; Pr_t = \frac{\overline{\rho u' v'}(\frac{\partial \overline{T}}{\partial y})}{\overline{\rho v' T'}(\frac{\partial \overline{u}}{\partial y})}, \tag{3.7}$$

$$R_{u'T'} = \frac{\overline{u'T'}}{\sqrt{\overline{u'^2}}\sqrt{\overline{T'^2}}} = -1, \; R_{u'v'} = -R_{v'T'}, \tag{3.8}$$

where R_{xy} denotes the correlation between x and y.

Although this set of relations has achieved some success for turbulent boundary layers with adiabatic walls, both extensive experiments (Debieve *et al.* 1982) and DNS data (Guarini *et al.* 2000) show that the total temperature fluctuation $\sqrt{\overline{T_t'^2}} \approx \sqrt{\overline{T'^2}}$ and thus is not negligible. In order to improve the SRA relation to account for the wall heat transfer and the total temperature fluctuations, by arguing that the characteristic length scales of the temperature fluctuations and the velocity fluctuations are similar, Gaviglio (1987) proposed a new SRA relation

$$\frac{\sqrt{\overline{T'^2}}}{\overline{T}} = (\gamma - 1)M^2 \frac{\sqrt{\overline{u'^2}}}{\overline{u}} \left(1 - \frac{\partial \bar{T}_t}{\partial \bar{T}}\right)^{-1}. \tag{3.9}$$

This equation (named GSRA) relates the intensity of the velocity temperature fluctuations, and it reduces to Eq. (3.7) when the total temperature is constant across the boundary layer. On the basis of a mixing-length model, Huang *et al.* (1995) proposed

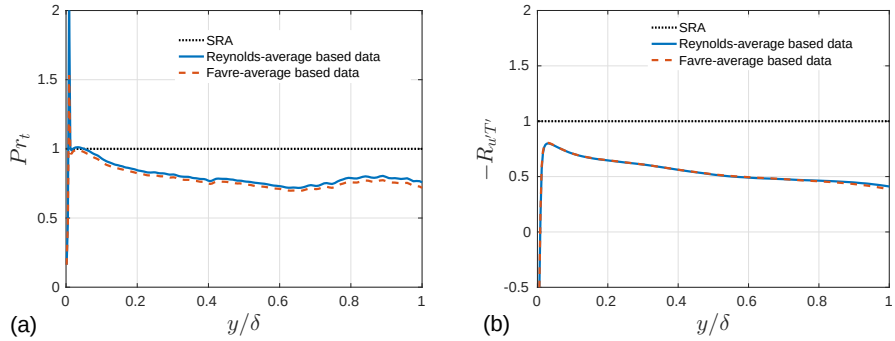

FIGURE 5. Assessment of the turbulent boundary layer at the streamwise station $(x - x_o)/\delta_o^\star = 580$ for $\alpha = 7°$: the distributions of the turbulent Prandtl number Pr_t (a) and the fluctuation correlation $-R_{u'T'}$ (b).

another new relation (commonly referred to as HSRA)

$$\frac{\sqrt{\overline{T'^2}}}{\overline{T}} = (\gamma - 1)M^2 \frac{\sqrt{\overline{u'^2}}}{\overline{u}} \left(1 - \frac{\partial \bar{T}_t}{\partial \bar{T}}\right)^{-1} / Pr_t, \tag{3.10}$$

which incorporates the effects of the local turbulent Prandtl number. Improvement over the original SRA has been verified for compressible turbulent channel flows (Huang *et al.* 1995) as well as for compressible turbulent boundary layers (Duan 2011).

As shown in Figure 5, the statistics of the turbulent Prandtl number Pr_t and the fluctuation correlation $R_{u'T'}$ are not sensitive to Favre- or Reynolds-average-based assessment. The turbulent Prandtl number varies between 0.7 and 1.0 across the boundary layer. Furthermore, the temperature fluctuation T' and the velocity fluctuation u' are not perfectly anti-correlated because Eq. (3.8) is derived by assuming a zero total temperature fluctuation; instead, it reaches values of approximately 10% for the present case. Note also that the correlation between T' and u' changes sign due to the non-monotonicity of the mean temperature profile in the near-wall regions.

Figure 6 shows the assessment of the turbulent boundary layer with SRA for $\alpha = 6°$, $7°$, and $8°$. The theoretical relations of SRA, GSRA, and HSRA are verified against the DNS data. The ratios of the left-hand sides of these relations to their right-hand sides are plotted for easy comparison, so the validity of a SRA relation implies that the plotted indicator is unity. For all three cases, the classical SRA relation fails to collapse to the DNS data across the boundary layers, similar to the observations of Duan *et al.* (2010) and Zhang *et al.* (2014) for high-Mach-number simulations over cold walls. While GSRA shows significant improvement over classical SRA, there is a 10% error even for the inner portion of the boundary layer. This deviation in the near-wall region is further reduced by the HSRA relation, which, however, still shows large discrepancies for the outer portion of the boundary layer. Excellent agreement is observed when the HSRA model is used with a constant turbulent Prandtl number $Pr_t = 0.9$.

Figure 7 plots the Reynolds stress $-\overline{\rho u'v'}$, the mean viscous shear stress $\overline{\mu}(\partial\overline{u}/\partial\overline{y})$, and the total shear stress for different wedge angles. While there is a narrow region with almost constant total shear stress in $y^+ < 40$, it decays at $y^+ > 40$ due to the effect of low Re_τ, and the decay rate agrees with the prediction by Chen *et al.* (2019). This decay induces built-in modeling errors for WMLES, which typically assume a constant total shear stress distribution inside the turbulent boundary layer.

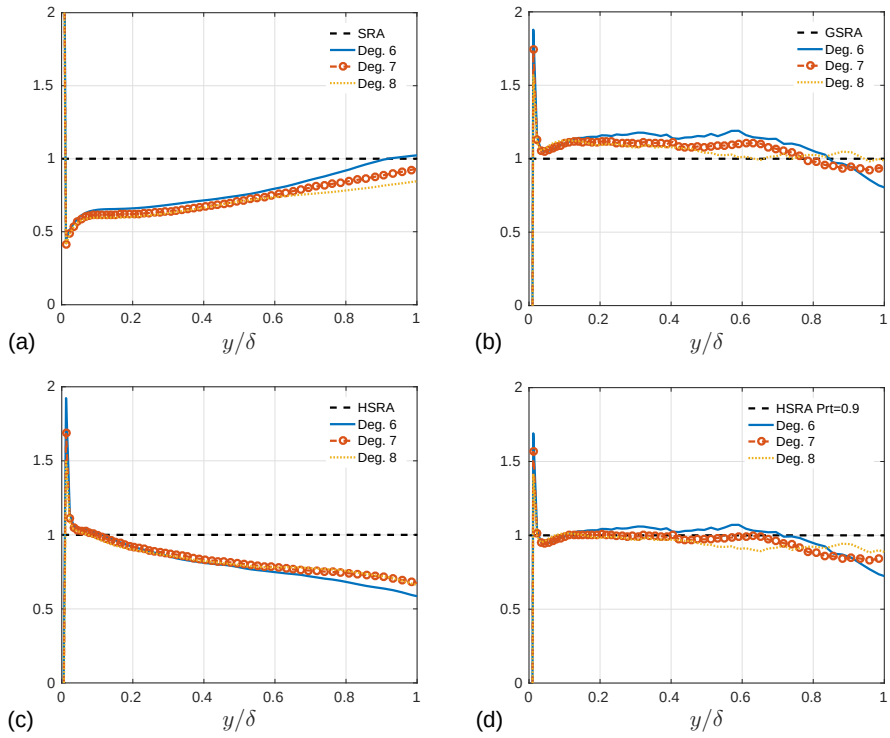

FIGURE 6. Assessment of the turbulent boundary layer at the streamwise station $(x - x_o)/\delta_o^\star = 580$ for $\alpha = 6°$, $7°$, and $8°$: the theoretical relations of SRA (a), GSRA (b), the original HSRA with local turbulent Prandtl number (c), and HSRA with constant turbulent Prandtl number $Pr_t = 0.9$ (d).

3.4. *Strong Reynolds analogy in transitional regions*

Since our simulations contain the entire transition process (for details, see Fu *et al.* 2018) it is useful to examine the turbulence statistics in the transitional boundary layer downstream of the shock-impingement location. A comparison between several profiles in the transitional region at $(x-x_o)/\delta_o^\star = 420, 460, 500$ and the fully turbulent region at $(x-x_o)/\delta_o^\star = 570$ is presented in Figure 8 for a fixed wedge angle of $\alpha = 7°$. The correlation between the streamwise velocity fluctuation u' and the temperature fluctuation T' is shown in Figure 8(a), the HSRA based on the local turbulent Prandtl number is shown in Figure 8(b), and the turbulent Prandtl number is shown in Figure 8(c). While significant variation in the concerned quantities is observed for the upstream station $(x - x_o)/\delta_o^\star = 420$, where the streaks break down dramatically, reasonably good collapse of the profiles for other stations is observed, at least for $y/\delta < 0.5$. Nevertheless, the fluctuation and deviation in Prandtl number pose significant challenges for determining the effective turbulent Prandtl number when the WMLES approach is employed for this type of transitional flow.

3.5. *Turbulence intensities*

In contrast to the case of subsonic turbulent flows, where the near-wall turbulence scales with the friction velocity u_τ and the length scale δ, Morkovin (1962) proposes that the velocity scale for high-speed turbulent stresses should be the density-weighted velocity

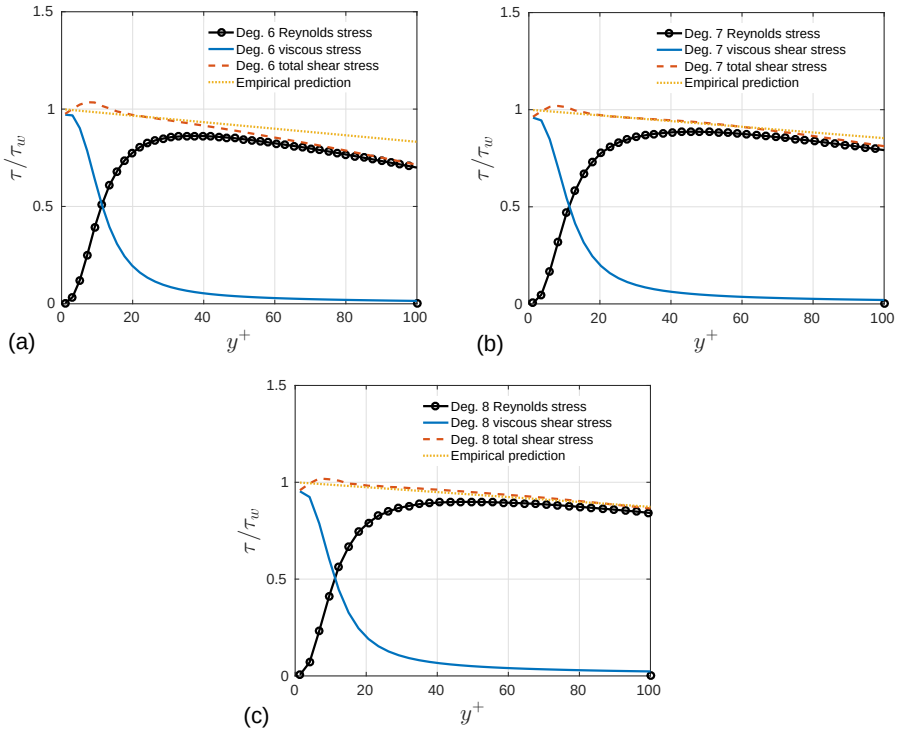

FIGURE 7. Assessment of the turbulent boundary layer at the streamwise station $(x - x_o)/\delta_o^\star = 580$: the distributions of the stress for $\alpha = 6°$ (a), $7°$ (b), and $8°$ (c). The empirical prediction denotes $\tau/\tau_w = 1 - y^+/Re_\tau$ for total shear stress in Chen *et al.* (2019).

scale $u_* = \sqrt{\tau_w/\rho}$. The experiment by Kistler (1959) confirms that the streamwise turbulence intensity collapses up to Mach number 4.7. A more recent comprehensive study of the available experimental data is presented by Williams *et al.* (2018), and a study of the available DNS data is presented by Zhang *et al.* (2018). However, the existing experimental data show a large scatter (see Figures 1 and 2 of Williams *et al.* 2018). The experimental uncertainties may come from the techniques used to measure the near-wall turbulent statistics with hot-wire anemometry and to perform the data analysis (e.g., the use of the SRA relation). Nonetheless, the fluctuating streamwise velocities in the outer boundary layer show a strong similarity to those of incompressible flows at comparable Reynolds numbers with Morkovin's scaling (Zhang *et al.* 2018; Williams *et al.* 2018).

Figures 9–11 show the distributions of transformed turbulence intensity u'_{rms}/u_*, v'_{rms}/u_*, and w'_{rms}/u_* versus wall-normal distance normalized by different length scales for three wedge angles. With the boundary layer thickness δ as the reference length scale (Figure 9), the distributions of turbulence intensity show remarkable scatter for the inner boundary layer. On the basis of the y^+ unit (Figure 10), the profiles collapse well in the near-wall regions but deviate significantly in the outer portion of the boundary layer. In contrast, excellent collapse is observed across the entire boundary layer with semilocal scaling for all three cases (Figure 11). As shown by Modesti & Pirozzoli (2016), the effect of the Reynolds number on the transformed profile of turbulence intensity is not negligible. A comparison between the present DNS data and a low-Mach-number reference

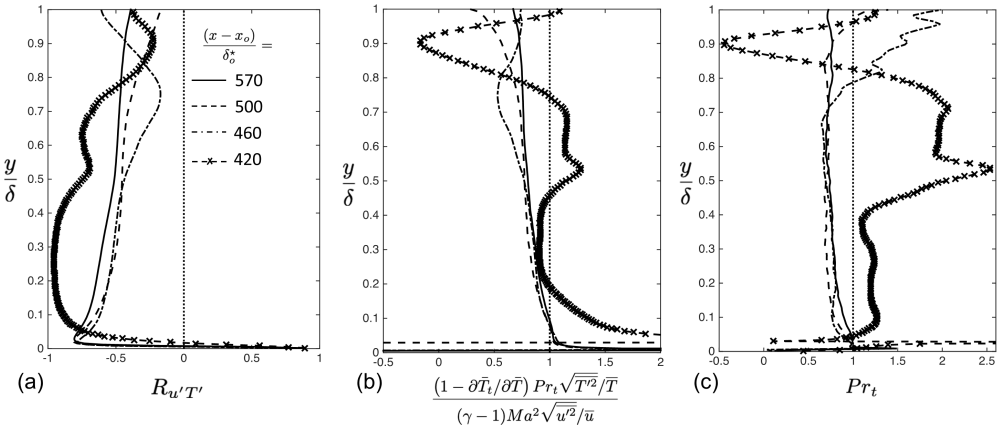

FIGURE 8. Wall-normal profiles at several streamwise stations for $\alpha = 7°$: temperature/streamwise-velocity correlation coefficient (a), modified strong Reynolds analogy (Huang *et al.* 1995) based on local turbulent Prandtl number (b), and turbulent Prandtl number (c).

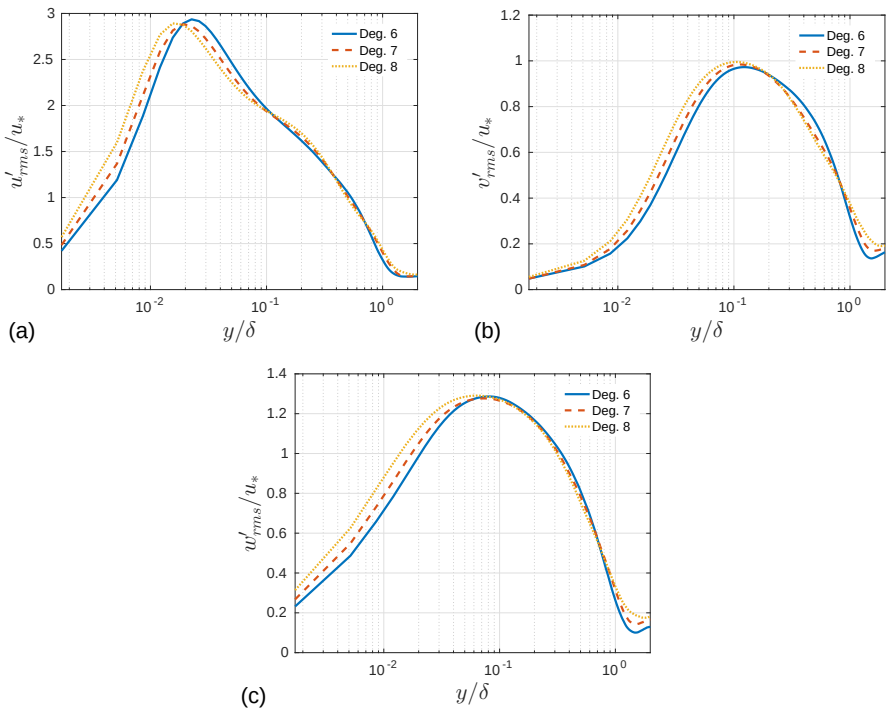

FIGURE 9. Turbulence intensities at the streamwise station $(x - x_o)/\delta_o^\star = 580$ for $\alpha = 6°$, $7°$, and $8°$ as a function of scaled wall-normal distance y/δ: u'_{rms}/u_* (a), v'_{rms}/u_* (b), and w'_{rms}/u_* (c).

with similar Re_τ (Modesti & Pirozzoli 2016) yields excellent agreement, especially for the streamwise velocity component, as can be seen in Figure 11.

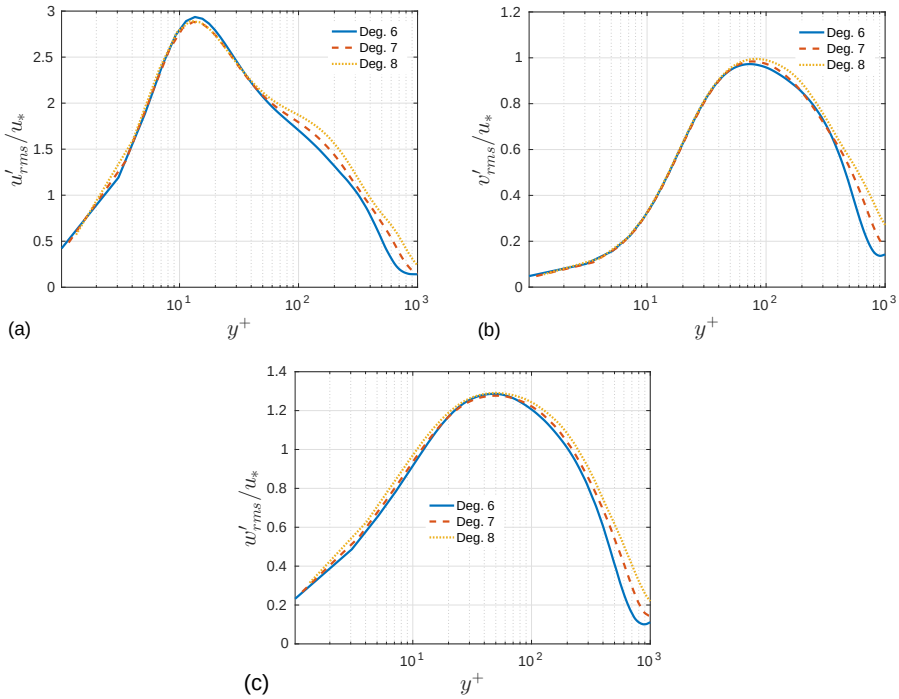

FIGURE 10. Turbulence intensities at the streamwise station $(x - x_o)/\delta_o^\star = 580$ for $\alpha = 6°$, $7°$, and $8°$ as a function of scaled wall-normal distance y^+: u'_{rms}/u_* (a), v'_{rms}/u_* (b), and w'_{rms}/u_* (c).

3.6. *Anisotropy effects*

Figure 12 shows the statistics of the anisotropy ratio w'_{rms}/u'_{rms}, v'_{rms}/u'_{rms}, and the structure parameter $-\overline{u'v'}/\overline{u'_iu'_i}$. For all three cases, the ratios are $w'_{rms}/u'_{rms} \approx 0.7$ and $v'_{rms}/u'_{rms} \approx 0.6$, both of which are within the range of incompressible turbulent boundary layers (Smits & Dussauge 2006; Duan 2011) although the present wall is cold. The turbulence structure parameter varies between 0.11 and 0.15, which is slightly lower than that of incompressible flows in the outer portion of the boundary layer.

4. Conclusions

In the present study, DNS of transitional shock/boundary layer interactions are utilized to examine the turbulent statistics in highly supersonic boundary layers. Three wedge angles are considered with an isothermal cold wall condition. The conclusions are as follows. First, for the mean velocity profile, both conventional transformations fail to collapse the compressible profiles to the log-law in the incompressible limit. The stronger the wall cooling is, the smaller is the effective von Kármán constant of the expected log profiles. Second, in terms of the mean temperature-velocity relation, Walz's model (Walz 1962) improves the prediction from the Crocco-Busemann formula (Crocco 1932; Busemann 1931) by further accounting for the effects of the non-unity Prandtl number but still generates remarkable deviations from DNS with a cold wall condition. In contrast, the prediction by Duan & Martin (2011) shows excellent agreement with DNS for all wedge angles. Third, both GSRA (Gaviglio 1987) and HSRA (Huang *et al.* 1995) improve the

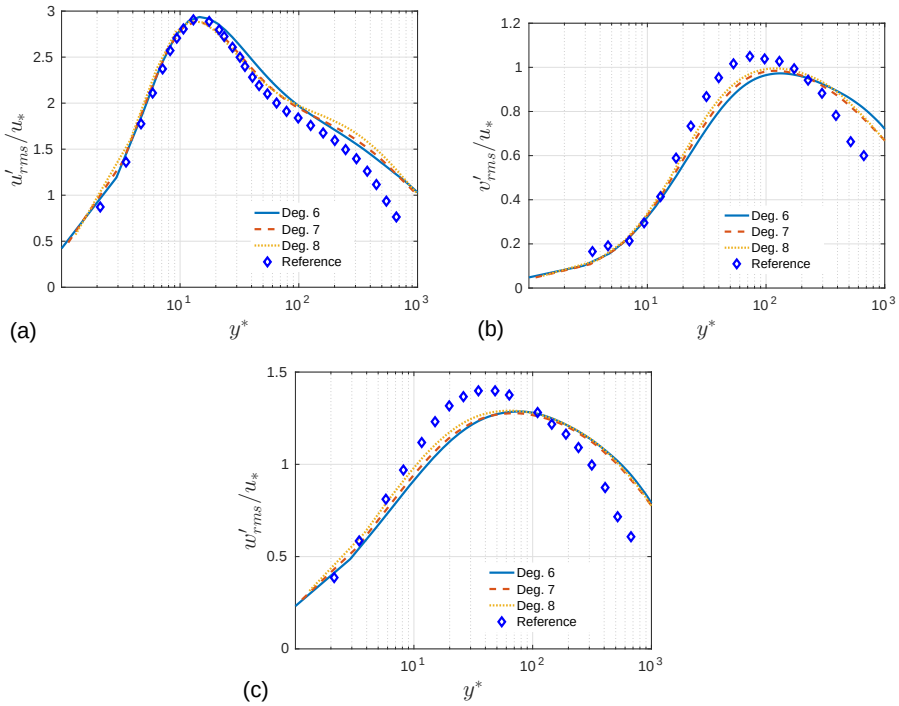

FIGURE 11. Turbulence intensities at the streamwise station $(x - x_o)/\delta_o^\star = 580$ for $\alpha = 6°$, $7°$, and $8°$ as a function of scaled wall-normal distance y^*: u'_{rms}/u_* (a), v'_{rms}/u_* (b), and w'_{rms}/u_* (c). The reference indicates the data of channel case CH15C ($Re_\tau = 1015$ and $Ma = 1.5$) from Modesti & Pirozzoli (2016).

prediction of the relation between the root mean square (rms) of the streamwise velocity fluctuation and the rms of the temperature fluctuation in comparison to SRA (Morkovin 1962). However, the best agreement comes from a modified HSRA model with a constant turbulent Prandtl number of 0.9 rather than the local Prandtl number in the original HSRA (Huang *et al.* 1995). Fourth, with the velocity scale proposed by Morkovin (1962) and semilocal scaling, the transformed turbulence intensities from three wedge angles collapse well to a low-Mach-number reference with a similar Reynolds number. Finally, despite the present high Mach number in the free stream, the statistics of the anisotropy ratio w'_{rms}/u'_{rms} and v'_{rms}/u'_{rms} show a similar distribution to that of an incompressible boundary layer.

Acknowledgments

This work was funded by the US Air Force Office of Scientific Research (AFOSR), Grant No. 1194592-1-TAAHO. Supercomputing resources were provided by the US Department of Energy through the INCITE Program. The authors are grateful to Dr. Jeffrey O'Brien, Dr. Christopher Ivey, and Dr. Minjeong Cho for useful discussions.

REFERENCES

BUSEMANN, A. 1931 *Handbuch der experimentalphysik*, **4**. Geest und Port.

BRES, G. A., BOSE, S. T., EMORY, M., HAM, F. E., SCHMIDT, O. T., RIGAS, G.

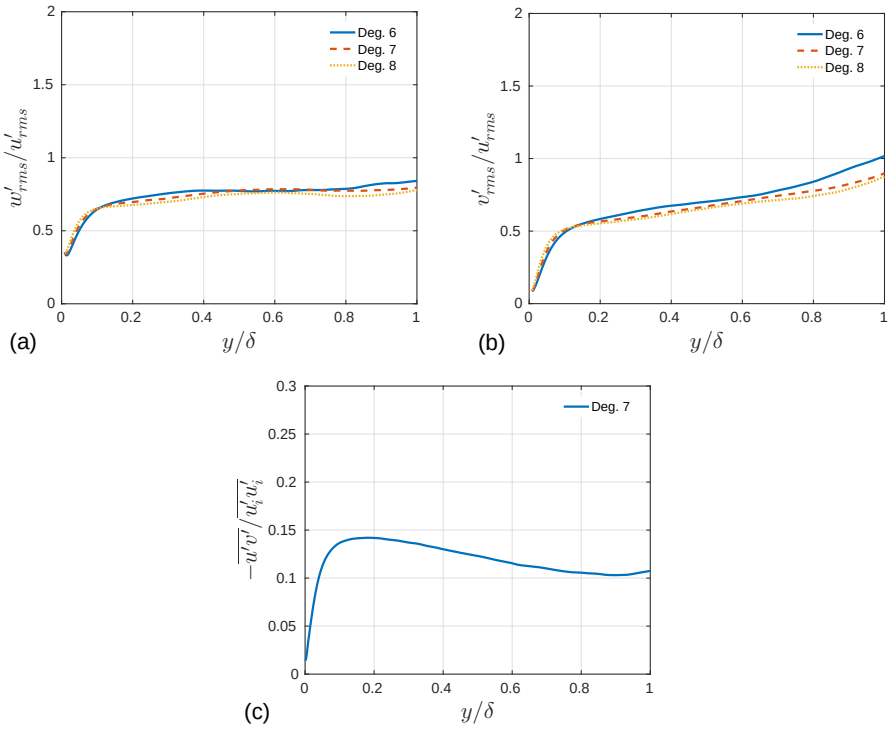

FIGURE 12. Turbulence statistics at the streamwise station $(x - x_o)/\delta_o^\star = 580$ for $\alpha = 6°$, $7°$, and $8°$: w'_{rms}/u'_{rms} (a), v'_{rms}/u'_{rms} (b), and the structure parameter $-\overline{u'v'}/\overline{u'_iu'_i}$ (c).

& COLONIUS, T. 2018 Large-eddy simulations of co-annular turbulent jet using a Voronoi-based mesh generation framework. *AIAA Paper* 2018-3302.

BOSE, S. T. & PARK, G. I. 2018 Wall-modeled large-eddy simulation for complex turbulent flows. *Annu. Rev. Fluid Mech.* **50**, 535–561.

CROCCO, L. 1932 Sulla trasmissione del calore da una lamina piana a un fluido scorrente ad alta velocita. *L'Aerotecnica* **12**, 181–197.

CHEN, X., HUSSAIN, F. & SHE, Z. S. 2019 Non-universal scaling transition of momentum cascade in wall turbulence. *J. Fluid Mech.* **871**, R2.

DUAN, L. 2011 *DNS of hypersonic turbulent boundary layers.* PhD thesis, Princeton University.

DUAN, L., BEEKMAN, I. & MARTIN, M. 2010 Direct numerical simulation of hypersonic turbulent boundary layers. Part 2. Effect of wall temperature. *J. Fluid Mech.* **655**, 419–445.

DUAN, L., BEEKMAN I. & MARTIN, M. 2011 Direct numerical simulation of hypersonic turbulent boundary layers. Part 3. Effect of Mach number. *J. Fluid Mech.* **672**, 245–267.

DEBIEVE, J. F., GOUIN, H. & GAVIGLIO J. 1982 Momentum and temperature fluxes in a shock wave-turbulence interaction. In *Structure of Turbulence in Heat and Mass Transfer,* ed. Zaric, Z. P., pp. 277–296. Hemisphere.

DUAN, L. & MARTIN, M. 2011 Direct numerical simulation of hypersonic turbulent boundary layers. Part 4. Effect of high enthalpy. *J. Fluid Mech.* **684**, 25–59.

Fernholz, H. H. & Finley, P. J. 1980 A critical commentary on mean flow data for two-dimensional compressible boundary layers. *AGARD-AG-253*.

Fu, L., Karp, M., Bose, S. T., Moin, P. & Urzay, J. 2018 Equilibrium wall-modeled LES of shock-induced aerodynamic heating in hypersonic boundary layers. *Annual Research Briefs*, Center for Turbulence Research, Stanford University, pp. 171–181.

Gaviglio, J. 1987 Reynolds analogies and experimental study of heat transfer in the supersonic boundary layer. *Int. J. Heat Mass Transf.* **30**, 911–926.

Guarini, S. E., Moser, R. D., Shariff, K. & Wray, A. 2000 Direct numerical simulation of a supersonic turbulent boundary layer at Mach 2.5. *J. Fluid Mech.* **414**, 1–33.

Huang, P., Coleman, G. & Bradshaw P. 1995 Compressible turbulent channel flows: DNS results and modelling. *J. Fluid Mech.* **305**, 185–218.

Kistler, A. L. 1959 Fluctuation measurements in a supersonic turbulent boundary layer. *Phys. Fluids* **2**, 290–296.

Morkovin, M. V. 1962 Effects of compressibility on turbulent flows. In *Mécanique de la Turbulence*, ed. Favre, A., pp. 365–380. CNRS.

Modesti, D. & Pirozzoli, S. 2016 Reynolds and Mach number effects in compressible turbulent channel flow. *Int. J. Heat Fluid Fl.* **59**, 33–49.

Pirozzoli, S., Grasso, F. & Gatski, T. B. 2004 Direct numerical simulation and analysis of a spatially evolving supersonic turbulent boundary layer at M=2.25. *Phys. Fluids* **16**, 530–545.

Reynolds, O. 1874 On the extent and action of the heating surface of steam boilers. *Int. J. Heat Mass Transf.* **3**, 163–166.

Smits, A. J. & Dussauge, J. P. 2006 *Turbulent Shear Layers in Supersonic Flow.* Springer Science & Business Media.

Sandham, N., Schülein, E., Wagner, A., Willems, S. & Steelant, J. 2014 Transitional shock-wave/boundary-layer interactions in hypersonic flow. *J. Fluid Mech.* **752**, 349–382.

Trettel, A. & Larsson, L. 2016 Mean velocity scaling for compressible wall turbulence with heat transfer. *Phys. Fluids* **28**, 026102.

Urzay, J. 2018 Supersonic combustion in air-breathing propulsion systems for hypersonic flight. *Annu. Rev. Fluid Mech.* **50**, 593–627.

van Driest, E. 1956 The problem of aerodynamic heating. *Aeronaut. Eng. Rev.* **15**, 26–41.

Volpiani, P. S., Bernardini, M. & Larsson, J. 2018 Effects of a nonadiabatic wall on supersonic shock/boundary-layer interactions. *Phys. Rev. Fluids* **3**, 083401.

Walz, A. 1962 Compressible turbulent boundary layers. *CNRS*, pp. 299–350.

Williams, O. J., Sahoo, D., Baumgartner, M. L. & Smits, A. J. 2018 Experiments on the structure and scaling of hypersonic turbulent boundary layers. *J. Fluid Mech.* **834**, 237–270.

Zhang, Y. S., Bi, W. T., Hussain, F. & She, Z. S. 2014 A generalized Reynolds analogy for compressible wall-bounded turbulent flows. *J. Fluid Mech.* **739**, 392–420.

Zhang, C., Duan, L. & Choudhari, M. M. 2018 Direct numerical simulation database for supersonic and hypersonic turbulent boundary layers. *AIAA J.* **56**, 4297–4311.